

RESEARCH ARTICLE

Comparative analysis of steel arch bridges under near-fault ground motion effects of directivity-pulse and fling-step

D. Yılmaz, K. Soyluk*

Gazi University, Department of Civil Engineering, Ankara, Turkey

Abstract

In this study, it is intended to investigate specifically the directivity-pulse and fling-step characteristics of near-fault ground motions on deck-type steel arch bridges. As known, near-fault ground motions have different dynamic characteristics than far-fault ground motions characterized by directivity pulse and fling step effects which usually have important effects on structural systems. The New River Gorge Bridge constructed in the USA is selected as a numerical example to determine the response of this type of steel arch bridges under the specified characteristics of near-fault ground motions. As near-fault ground motions 1999 Chi-Chi Earthquake strong ground motion recordings of TCU102, TCU089 and HWA032 are used. The bridge responses obtained for the near-fault ground motions showing directivity-pulse and fling-step characteristics are compared with each other and with those of the responses obtained for the far-fault ground motion to emphasize the relative importance of directivity-pulse and fling-step effects. The results revealed that both directivity-pulse and fling-step characteristics of near-fault ground motions have considerable effects on steel arch bridge responses and therefore should be taken into account in the design phase of these bridges.

Keywords

Deck-type Steel arch bridge; Near-fault ground motion; Directivity-pulse effect; Fling-step effect; Far-fault ground motion

Received: 18 May 2019; Accepted: 20 June 2019

ISSN: 2630-5763 (online) © 2019 Golden Light Publishing® All rights reserved.

1. Introduction

Near-fault ground motions are different from ordinary ground motions in that they often contain strong coherent dynamic long period pulses and permanent ground displacements. The dynamic motions are dominated by a large long period pulse of motion that occurs on the horizontal component perpendicular to the strike of the fault, caused by rupture directivity (directivity-pulse) effects. The static ground displacements in near-fault ground motions are caused by the relative movement of the two sides of the fault on which the earthquake

occurs (fling-step effect). These displacements are discontinuous across a fault having surface rupture, and can subject a bridge crossing a fault to significant differential displacements. The static ground displacements occur at about the same time as the large dynamic motions, indicating that the static and dynamic displacements need to be treated as coincident loads. These dynamic motions and static ground displacements are defined by “directivity-pulse” and “fling step” effects [1]. If compared with the far-fault ground motions, the long-period and high-density directivity-pulse effect and the fling-step effect causing permanent

* Corresponding author
E-mail: ksoyluk@gazi.edu.tr

static ground displacements, can be observed as the destructive characteristics of near-fault ground motions.

In the literature it is possible to find several studies conducted on bridge type structural systems to determine the seismic responses of bridges under near fault ground motions. The previously published papers about highway bridges and viaducts [2-9] and cable-supported bridges [10-17] revealed that near fault ground motions with directivity-pulse and fling-step characteristics cause larger seismic demands on bridges with respect to the far-fault ground motions. Although many studies have been performed to determine the seismic responses of bridges under near fault ground motions so far, studies investigating the seismic responses of steel arch bridges under near-fault ground motions with directivity-pulse and fling-step characteristics are rather limited. Yan et al. [18] investigated the seismic response of a steel tied half through arch bridge (Lupu Bridge) under near-field ground motions and concluded that the selected near-fault ground motions cause larger responses of the major components of the bridge. Yan and Lee [19] investigated steel arch bridges under near-fault ground motions by emphasizing the travelling wave effect of the selected near-fault ground motions. The effects of fling step and long period pulses on the bridge responses were also discussed. Liu and Zhang [20] focused on the impact of the wave passage effect on long-span arch bridges under ground motion records selected from near-fault motions. It was shown that the seismic damages are increased by the wave passage effect and the increase is more obvious for near-fault ground motions. Recently Yilmaz and Soyuluk [21] conducted dynamic time history analysis of a steel arch bridge for near fault ground motions showing directivity pulse and fling-step characteristics as an initial study of this paper.

Because arch bridges are also started to be used to pass longer spans which is mainly dominated by cable-supported bridges, it has become important to determine the dynamic behavior of this type of bridges under ground motions showing near fault

characteristics. Therefore, in this study it is intended to perform dynamic time history analyses of steel arch bridges specifically for near-fault ground motions showing directivity pulse and fling-step characteristics.

2. Selected ground motions

The most distinctive effects of near fault ground motions are the directivity pulse and fling step effects. Near-fault ground motions show pulse like characteristics at the initial phase of the ground motions and have pulse durations usually larger than 2-3 seconds (forward-directivity effect). The fling-step effect which results permanent ground displacements should also be taken into account as another important property of near fault ground motions. In this study far-fault and near-fault ground motion components of Chi-Chi earthquake is used to investigate the forward-directivity and fling-step effects on steel arch bridges. The recordings of Chi-Chi earthquake used in this study are mainly obtained from the Pacific Earthquake Engineering Research Center (PEER) at <https://peer.berkeley.edu/peer-strong-ground-motion-databases>. Also, raw recordings of this earthquake are obtained from Prof. David M. Boore [22]. The recordings of HWA032, TCU089 and TCU102 ground motion components are used in this study to determine the responses of the considered steel arch bridge under far-fault and near-fault ground motions.

Because the distance between the station where the TCU102 component is recorded and the location of the fault is 1.49 km, it is accepted as a near fault ground motion. The east-west component of TCU102 recording obtained through the PEER Strong Motion Database is used as near fault ground motion showing directivity pulse characteristics. The directivity pulse characteristics can be noticed in the velocity-time history graph (Fig. 1b). In the east-west component of TCU102 recording, PGA is measured as 0.30 g and PGV as 91.3 cm/s (Fig. 1).

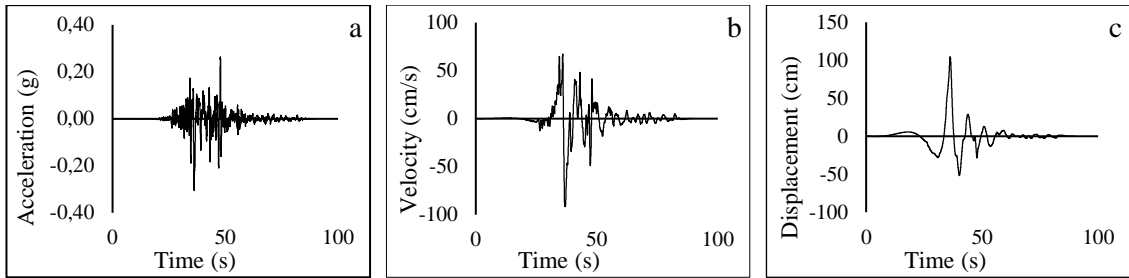


Fig. 1. a) Acceleration, b) Velocity, c) Displacement; time history plots of TCU102 recording in the east-west direction

The displacement time histories obtained through the PEER Strong Motion Database do not show static displacements due to the applied standard data processing procedures [23]. Therefore, to investigate the fling-step effect, raw recordings are required so that displacement-time history recordings showing static displacements can be obtained. Integrations are performed through the raw acceleration-time history plot of the north-south component of TCU102 recording obtained from Boore [22] (Fig. 2a) to get the velocity-time and displacement-time history plots. But due to the technical reasons related to the sensitivity of the instruments and secondary vibrations in the environment, the velocity obtained by the integration of the recording do not come to rest at the end of the motion (Fig. 2b). Considering the fact that the velocity does not come to rest towards the end of the motion, it becomes necessary to apply a correction to the recording. Therefore, a baseline correction procedure is applied to the velocity-time history plot which is determined from the integration of the acceleration-time history graph so that velocity-time history plot with zero ending is obtained (Fig. 2c). Then, this velocity-time history plot is integrated once more to get the displacement-time history with permanent ground displacements (Fig. 3). In the north-south component of TCU102 recording, PGA is measured as 0.17 g and PGV as 64.4 cm/s. As a result of fling-step effect, 126 cm ground displacement is obtained at the end of the record (Fig. 3).

Because the distance between the station where the TCU089 component is recorded and the location of the fault is 9 km, it is also accepted as a near fault motion. Although it is a near-fault ground

motion, it does not show any directivity pulse characteristics in the velocity-time history plots. In the east-west component of TCU089 recording, PGA is measured as 0.35 g and PGV as 35.2 cm/s (Fig. 4).

On the other hand, it can be noticed that the north-south component of TCU089 shows fling-step characteristics. For this ground motion component, PGA is measured as 0.24 g and PGV as 32.1 cm/s (Fig. 5). As a result of the fling-step effect, 64 cm static ground displacement is obtained at the end of the record (Fig. 6).

Considering the fact that HWA032 component of Chi-Chi earthquake is located 47.31 km from the fault, it is accepted as a far-fault motion. It is possible to observe that displacement- and velocity-time history graphs of HWA032 do not show any fling-step and directivity pulse characteristics, respectively. In the north-south component of HWA032 recording obtained from PEER, PGA is measured as 0.11 g and PGV as 8.3 cm/s (Fig. 7).

As a summary, while the displacement-time history plots for fling-step effect showing static displacements are obtained through the integration of the raw records (Figs. 3 and 6), the displacement-time history plots for directivity-pulse effect are obtained through the PEER Strong Motion Database (Figs. 1c, 4c and 7c).

The recordings of Chi-Chi earthquake which are used in this study are shown in Table 1 with signal parameters. While the near-fault recording TCU102-EW shows pulse type signals, TCU089-EW does not reflect any pulse type characteristics. On the other hand, TCU102-NS and TCU089-NS near-fault ground motion components show fling-step characteristics.

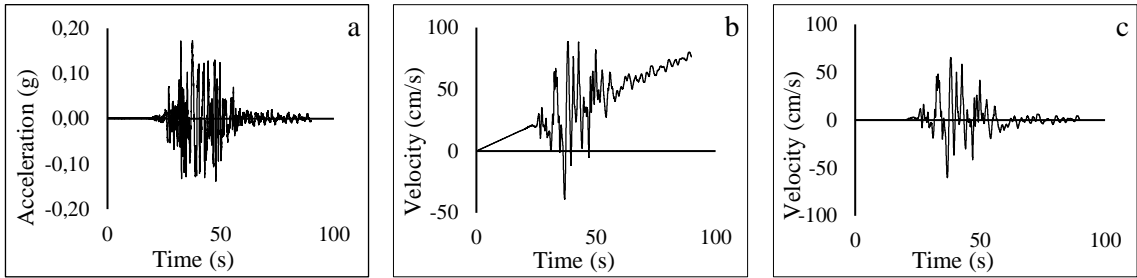


Fig. 2. a) Raw acceleration, b) Integrated velocity, c) Baseline corrected velocity; time history plots of TCU102 recording in the north-south direction

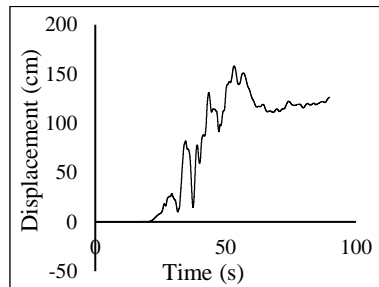


Fig. 3. Integrated displacement time history plot of TCU102 recording in the north-south direction

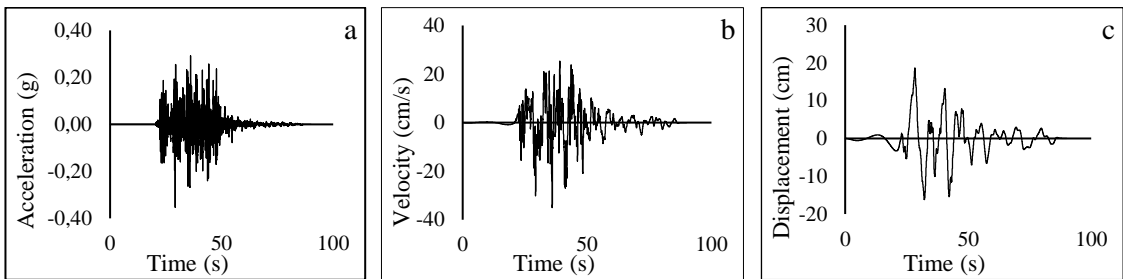


Fig. 4. a) Acceleration, b) Velocity, c) Displacement; time history plots of TCU089 recording in the east-west direction

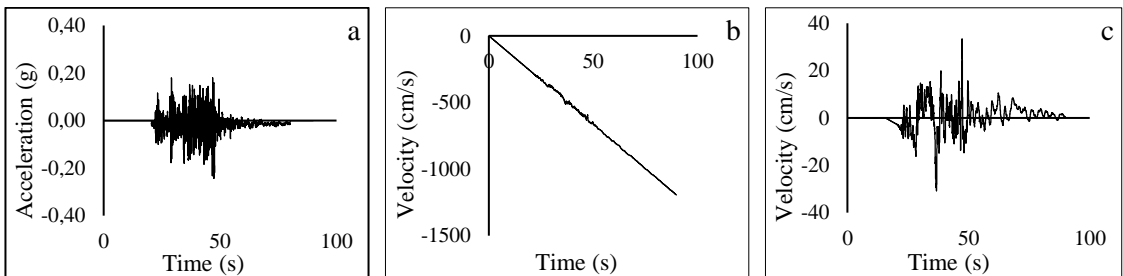


Fig. 5. a) Raw acceleration, b) Integrated velocity, c) Baseline corrected velocity; time history plots of TCU089 recording in the north-south direction

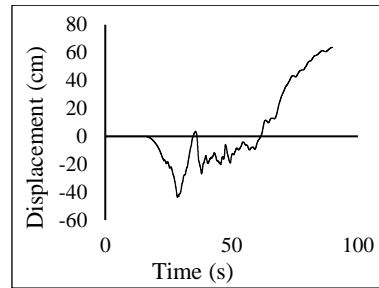


Fig. 6. Integrated displacement time history plot of TCU089 recording in the north-south direction

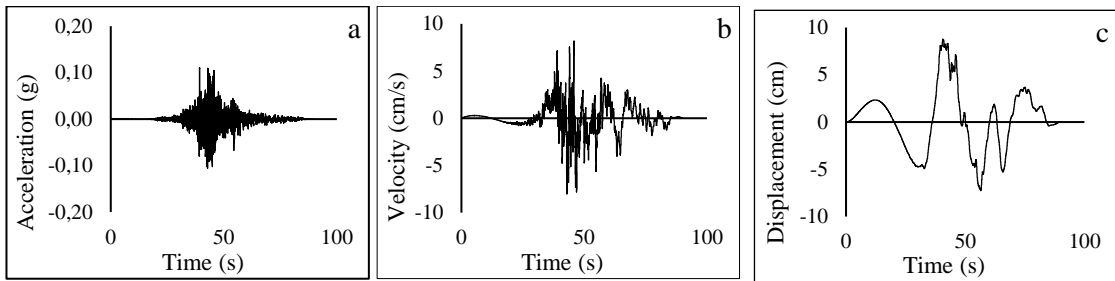


Fig. 7. a) Acceleration, b) Velocity, c) Displacement; time history plots of HWA032 recording in the north-south direction

Table 1. Ground motion characteristics

Record	Direction	Effect	d	PGA	PGV	PGV/PGA	Fling Step
			(km)	(g)	(cm/s)	(s)	(cm)
TCU102	NS	Fling Step	1.49	0.17	64.40	3.79	126
TCU102	EW	Directivity	1.49	0.30	91.30	3.04	-
TCU089	NS	Fling Step	9	0.24	33.07	0.14	64
TCU089	EW	No-Pulse	9	0.35	34.91	0.11	-
HWA032	NS	Far Fault	47.31	0.10	7.91	0.08	-

3. Modeling of the arch bridge

In this study, the New River Gorge Bridge (NRGB) located in the USA is considered as a deck-type arch bridge model (steel arch bridge with the roadway deck located above the arch). The New River Gorge Bridge is a box truss and steel deck arch bridge. Both the deck and the arch are essentially box trusses consisting of four box girder chords connected by lateral and vertical truss members. The NRGB has a north approach span of 175 m, a south approach of 193 m and a main span of 554 m. The approach span deck segments are isolated from the main span deck segments by expansion joints at the ends of the main span [24].

3D model of NRGB is used to determine the seismic responses of the bridge. The finite element model is represented by 1737 joints, 2576 beam elements and 48 link elements (Fig. 8).

4. Numerical calculations

In this study dynamic time history analyses of the considered arch bridge are conducted for the near-fault ground motion components of Chi-Chi earthquake with directivity pulse and fling-step effects (TCU102 and TCU089) and for the far-fault ground motion component of Chi-Chi earthquake (HWA032).

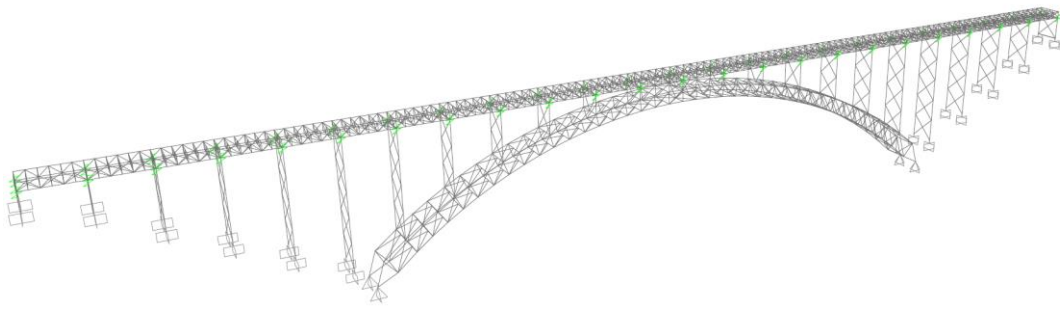


Fig. 8. 3D model of the New River Gorge Bridge

The ground motions are applied to the bridge system in the longitudinal direction in terms of displacement-time history records. For the modeling and dynamic analysis of the arch bridge, SAP2000V14.1 [25] structural analysis program is used and the resulting bridge responses are compared along the bridge deck and arch for the considered ground motion components.

Horizontal displacements obtained at the bridge deck for the considered near- and far-fault earthquake recordings are compared in Fig. 9a. It can be observed that TCU102-NS and TCU102-EW near fault ground motion components showing fling-step and directivity pulse characteristics, respectively, cause larger displacements than those of the near fault ground motion components of TCU089-NS, TCU089-EW and far fault ground motion component of HWA032. It can be noticed that while the maximum displacements are determined for the TCU102-NS component having fling-step effect at the center region of the deck, TCU102-EW component having directivity-pulse effect causes the maximum displacements at the side regions. If the ground motion components TCU089-NS and TCU089-EW which show fling-step and no-directivity pulse characteristics are considered it can be observed that TCU089-NS component which shows fling-step effect results generally larger displacements. As expected for the far-fault ground motion component HWA032, the smallest displacements are obtained. Although both near fault ground motions TCU102-NS and TCU089-NS show fling-step characteristics, the difference in the displacements obtained between these ground motions might be explained by the

fact that TCU102-NS ground motion component has larger peak ground velocity (64.40 cm/s) and static ground displacement (126 cm) than those of the TCU089-NS component (33.07 cm/s and 64 cm). If the displacements are compared at the deck point where maximum displacements are obtained, it can be observed that the displacement obtained for the TCU102-NS component causes 42%, 60%, 87% and 93% larger displacements than those of the TCU102-EW, TCU089-NS, TCU089-EW and HWA032 ground motion components, respectively.

Horizontal displacements obtained over the length of the bridge arch are compared in Fig. 9b. It can be observed that the maximum displacements are determined for the TCU102-NS component showing fling-step characteristics. In addition to this, TCU102-NS and TCU102-EW near fault ground motion components which show fling-step and directivity-pulse characteristics, respectively, cause much larger displacements than those of the near fault ground motion components of TCU089-NS and TCU089-EW. As the horizontal arch displacements obtained for TCU089-EW and TCU089-NS near fault ground motion components are very close to each other, the smallest displacements are obtained for the far fault ground motion component HWA032. If the displacements are compared at the deck point where maximum displacements are obtained, it can be noticed that the displacement obtained for the TCU102-NS component causes 37%, 80%, 83% and 96% larger displacements than those of the TCU102-EW, TCU089-NS, TCU089-EW and HWA032 ground motion components, respectively.

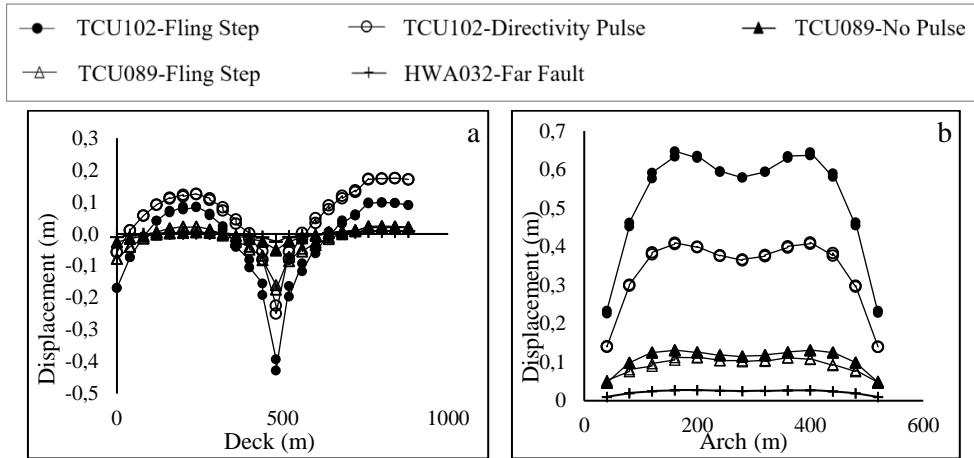


Fig. 9 (a) Horizontal; a) deck displacements (b) arch displacements

Vertical deck and arch displacements obtained for the bridge are compared in Fig. 10 for the earthquake recordings showing directivity-pulse and fling-step characteristics. It is possible to observe that the variation obtained for the vertical deck and arch displacements is consistent with the variation of horizontal displacements at the arch. Also, here the maximum displacements are determined for the TCU102-NS component showing fling-step characteristics. TCU102-NS and TCU102-EW near fault ground motion components which show fling-step and directivity-pulse characteristics, respectively, cause much larger displacements than those of the near fault ground motion components of TCU089-NS and TCU089-EW. As the vertical displacements obtained for TCU089-EW and TCU089-NS near fault ground motion components are very close to each other, the smallest displacements are obtained for the far fault ground motion component HWA032.

Bending moments obtained at the bridge deck are shown in Fig. 11a. It can be noticed that opposite to the deck and arch displacements TCU102-EW near-fault ground motion component showing directivity-pulse characteristics causes the largest bending moments. As the TCU102-NS component showing fling-step characteristics causes larger bending moments than those of the TCU089-NS and TCU089-EW near fault ground motions components, HWA032 far-fault ground

motion component causes the smallest bending moments. If the bending moments are compared at the arch point where maximum bending moments are obtained, it can be noticed that the bending moment obtained for the TCU102-EW component causes 70% larger bending moment than those of the TCU102-NS ground motion component.

From the comparison of the arch bending moments (Fig. 11b), it can be noticed that the largest bending moments are obtained for the TCU102-NS and TCU102-EW near-fault ground motion components. As the arch bending moments obtained for the TCU089-EW ground motion component showing fling-step characteristics results larger bending moments than those of the TCU089-NS near fault ground motion component showing no-directivity pulse characteristics, the smallest arch bending moments are obtained for the far fault ground motion component HWA032. If the bending moments are compared at the deck point where maximum bending moments are obtained, it can be noticed that the bending moment obtained for the TCU102-NS component causes 17% larger bending moment than those of the TCU102-EW ground motion component.

From the comparison of the deck axial forces (Fig. 12a), it can be noticed that the maximum axial forces are obtained for the TCU102-NS and TCU102-EW near-fault ground motion components.

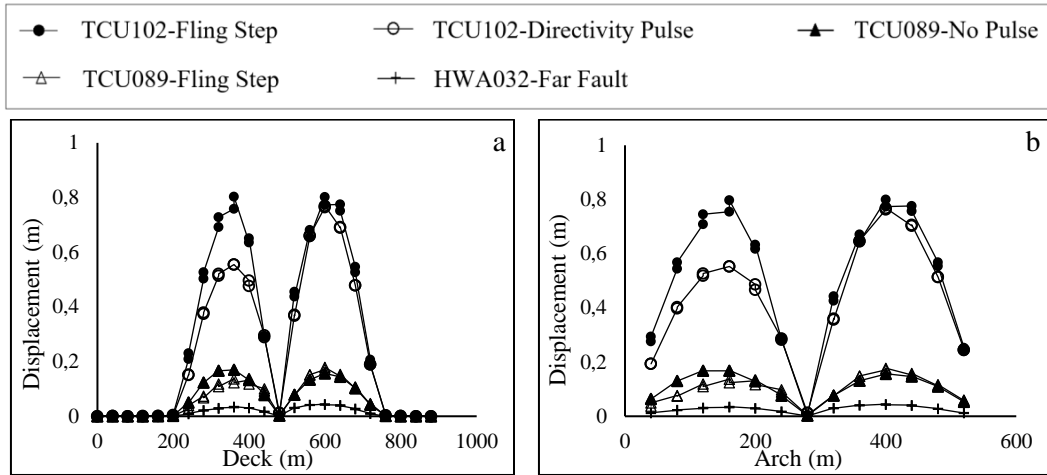


Fig. 10 Vertical; a) deck displacements (b) arch displacements

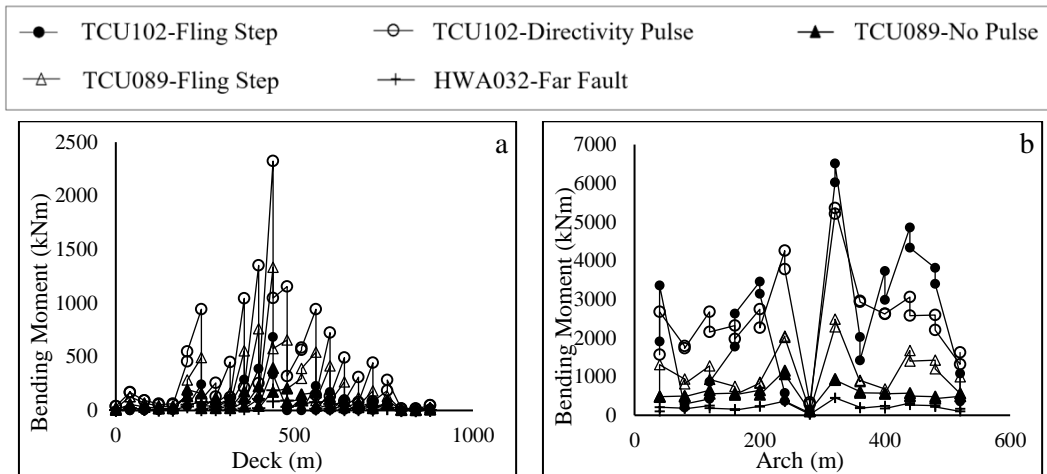


Fig. 11 Bending moments at the; a) deck (b) arch

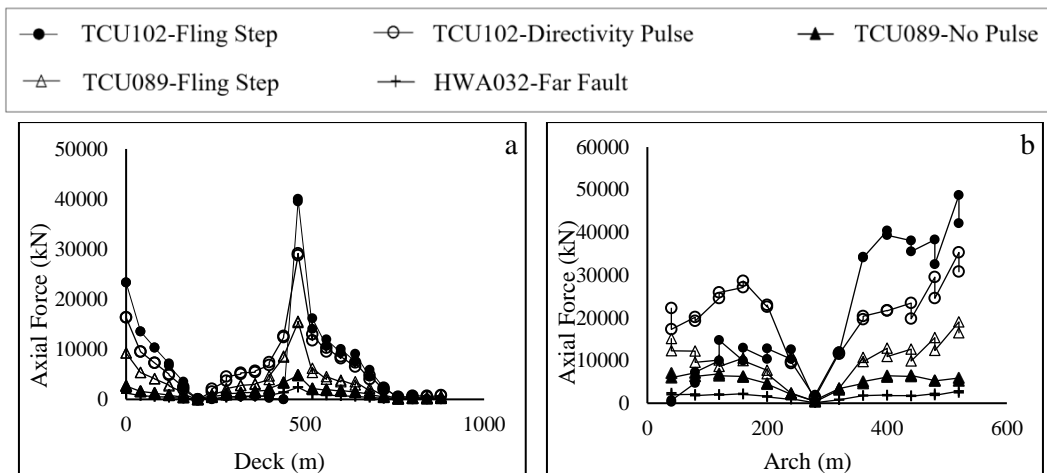


Fig. 12 Axial forces at the; a) deck (b) arch

If the ground motion components TCU089-NS and TCU089-EW which show fling-step and no-directivity pulse characteristics are compared, it can be observed that TCU089-NS component which shows fling-step effect results larger axial forces. As expected for the far-fault ground motion component HWA032, the smallest axial forces are obtained. If the axial forces are compared at the deck point where maximum axial forces are obtained, it can be noticed that the axial force obtained for the TCU102-NS component causes 27%, 62%, 88% and 94% larger axial forces than those of the TCU102-EW, TCU089-NS, TCU089-EW and HWA032 ground motion components, respectively.

Arch axial forces obtained over the length of the arch are compared in Fig. 12b. It can be noticed that while the maximum axial forces are determined for the TCU102-NS component having fling-step effect at one side of the arch, TCU102-EW component having directivity-pulse effect causes the maximum axial forces at the other side of the arch. If the ground motion components TCU089-NS and TCU089-EW which show fling-step and no-directivity pulse characteristics are considered it can be observed that TCU089-NS component which show fling-step effect results larger axial forces. As expected for the far-fault ground motion component HWA032, the smallest axial forces are

obtained. If the axial forces are compared at the arch point where maximum axial forces are obtained, it can be noticed that the axial force obtained for the TCU102-NS component causes 27% larger axial force than those of the TCU102-EW ground motion component.

From the comparison of the deck shear forces (Fig. 13a), it is possible to observe that the largest shear forces are determined for TCU102-NS component showing fling-step characteristics. In addition to this, TCU102-EW component showing directivity-pulse characteristics causes larger shear forces than those of the components of TCU089-NS and TCU089-EW. As the deck shear forces obtained for the TCU089-EW ground motion component showing fling-step characteristics results larger shear forces than those of the TCU089-NS component showing no-directivity pulse characteristics, the smallest shear forces are obtained for the component of HWA032 showing far-fault characteristics. If the shear forces are compared at the deck point where maximum shear forces are obtained, it can be noticed that the shear force obtained for the TCU102-NS component causes 28%, 61%, 88% and 94% larger shear forces than those of the TCU102-EW, TCU089-NS, TCU089-EW and HWA032 ground motion components, respectively.

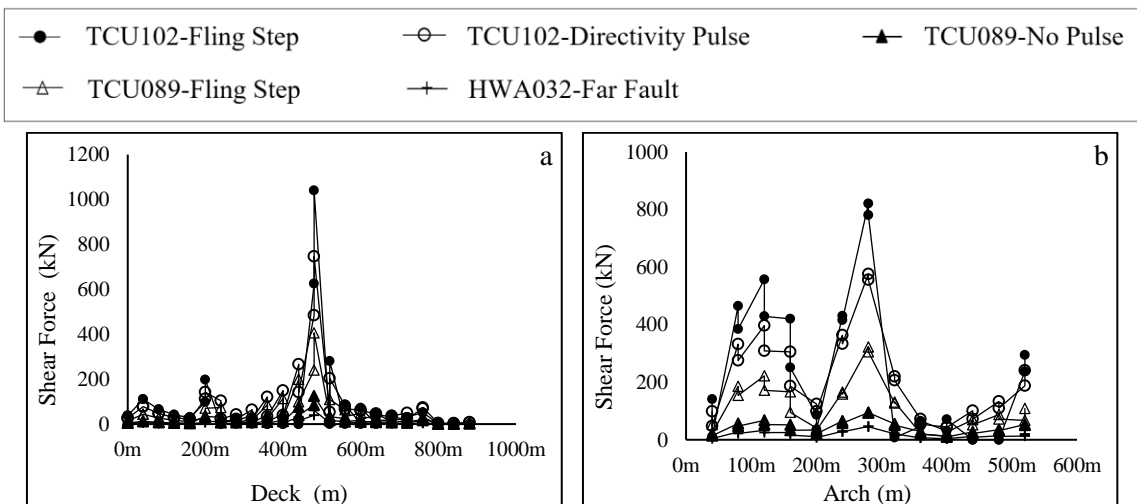


Fig. 13 Shear forces at the; a) deck (b) arch

From the comparison of the arch shear forces (Fig. 13b), it can be noticed that the largest shear forces are obtained for the TCU102-NS and TCU102-EW near-fault ground motion components. As the arch shear forces obtained for the TCU089-EW ground motion component showing fling-step characteristics results larger shear forces than those of the TCU089-NS component showing no-directivity pulse characteristics, the smallest arch shear forces are obtained for the component of HWA032 showing far-fault characteristics. If the shear forces are compared at the arch point where maximum shear forces are obtained, it can be noticed that the shear force obtained for the TCU102-NS component causes 29% larger shear force than those of the TCU102-EW ground motion component.

5. Conclusions

In this study, it is intended to investigate specifically the directivity-pulse and fling-step characteristics of near-fault ground motions on deck-type steel arch bridges. The New River Gorge Bridge constructed in the USA is selected as a numerical example to determine the responses of this type of steel arch bridges under the specified characteristics of near-fault earthquake motions. As near-fault earthquake motions 1999 Chi-Chi Earthquake strong motion records of TCU102, TCU089 and HWA032 are used. The bridge responses obtained for the near-fault ground motions showing directivity-pulse and fling-step characteristics are compared with each other and with those of the responses obtained for the far-fault ground motions to emphasize the relative importance of directivity-pulse and fling-step effects. The results revealed that:

- Maximum deck and arch displacements are generally obtained for TCU102-NS component having fling-step characteristics.
- -While the maximum member forces at the deck and arch are generally obtained for TCU102-NS component having fling-step characteristics, it is also possible to see that TCU102-EW component showing directivity-pulse

characteristics causes the most critical structural responses for some member forces.

- Near-fault ground motions result much larger response values than those of the far-fault ground motion.
- Although the member forces obtained for the ground motion component of TCU089-NS showing fling-step characteristics are usually larger than the corresponding member forces obtained for the TCU089-EW component showing no-directivity pulse characteristics, displacements obtained for both components are relatively close to each other.
- Although both TCU102-NS and TCU089-NS near fault ground motions show fling-step characteristics, the difference in the responses obtained between these ground motions can be attributed to the fact that TCU102-NS ground motion component has larger peak ground velocity and static ground displacement than those of the TCU089-NS component.

Depending on these results it can be concluded that directivity-pulse and fling-step characteristics of near fault ground motions have considerable effects on deck-type steel arch bridge responses. Especially the fling-step effect causing permanent static ground displacements, may have larger seismic demands on steel arch bridges. However, because the results are obtained just for a single steel arch bridge and for a couple of selected earthquake motions, the results should be verified with more arch bridge models and near-fault ground motions.

References

- [1] Somerville PG. Characterizing near fault ground motion for the design and evaluation of bridges. Proceedings of the 3rd National Seismic Conference and Workshop on Bridges and Highways, 137-148, 2002, Portland, USA.
- [2] Liao WI, Loh CH, Wan S, Jean WY, Chai JF (2000) Dynamics responses of bridges subjected to near-fault ground motions. Journal of the Chinese Institute of Engineers 23(4): 455-464.
- [3] Liao WI, Loh CH, Lee BH (2004) Comparison of dynamic response isolated and non-isolated continuous girder bridges subjected to near-fault

- ground motions. *Engineering Structures* 26: 2173-2183.
- [4] Park SW, Ghasemi H, Shen J, Somerville PG, Yen, WP, Yashinsky M (2004) Simulation of the seismic performance of the Bolu Viaduct subjected to near-fault ground motions. *Earthquake Engineering and Structural Dynamics* 33(13): 1249-1270.
- [5] Xinle L, Huijan D, Xi Z (2007) Engineering characteristics of near-fault vertical ground motions and their effect on the seismic response of bridges. *Earthquake Engineering and Engineering Vibration* 6(4): 345-350.
- [6] Jónsson M, Bessason B, Haflidason E (2010) Earthquake response of a base-isolated bridge subjected to strong near-fault ground motion. *Soil Dynamics and Earthquake Engineering* 30(6): 447-455.
- [7] Jalali RS, Jokandan MB, Trifunac MD (2012) Earthquake response of a three-span, simply supported bridge to near-field pulse and permanent-displacement step. *Soil Dynamics and Earthquake Engineering* 43: 380-397.
- [8] Yasrebi L, Ghafory-Ashtiany M (2014) Inelastic response of a long span bridge under asynchronous near-field pulse-like and far-field excitations. *Journal of Seismology and Earthquake Engineering* 16(2): 111-128.
- [9] Sevim B, Atamturktur S, Altunışık AC, Bayraktar A (2016) Ambient vibration testing and seismic behavior of historical arch bridges under near and far fault ground motions. *Bulletin of Earthquake Engineering* 14(1): 241-259.
- [10] McCallen DB, Astaneh-Asl A, Larsen SC, Hutchings LJ. Dynamic response of the suspension spans of the San Francisco-Oakland Bay Bridge. 8th U.S. National Conference on Earthquake Engineering, 2006, San Francisco, USA.
- [11] Jia J, Ou JP. Seismic analysis of long-span cable-stayed bridges subjected to near-fault pulse-type ground motions. The 14th World Conference on Earthquake Engineering, 2008, Beijing, China.
- [12] Adanur S, Altunışık AC, Bayraktar A, Akköse M (2012) Comparison of near-fault and far-fault ground motion effects on geometrically nonlinear earthquake behavior of suspension bridges. *Natural Hazards* 64(1): 593-614.
- [13] Shrestha B, Tuladhar R (2012) The response of Karnali Bridge, Nepal to near-fault earthquakes. *Bridge Engineering* 165(BE4): 223-232.
- [14] Ismail M, Casas JR, Rodellar J (2013) Near-fault isolation of cable-stayed bridges using RNC isolator. *Engineering Structures* 30: 327-342.
- [15] Shrestha B (2015) Seismic response of long span cable-stayed bridge subjected to near-fault vertical ground motions. *KSCE Journal of Civil Engineering* 19(1): 180-187.
- [16] Soyluk K, Karaca H (2017) Near-fault and far-fault ground motion effects on cable-supported bridges. *International Conference on Structural Dynamics, Procedia Engineering, EURO DYN 2017* 199: 3077-3082.
- [17] Li S, Zhang F, Wang JQ, Alam MS, Zhang J (2017) Seismic responses of super-span cable-stayed bridges induced by ground motions in different sites relative to fault rupture considering soil-structure interaction. *Soil Dynamics and Earthquake Engineering* 101: 295-310.
- [18] Yan X, Lee GC, Lichu G, Shide H (2006) A comparative study between China and U.S. on seismic design philosophy and practice of a long span arch bridge. *Earthquake Engineering and Engineering Vibration* 5(1): 61-69.
- [19] Yan X, Lee GC (2007) Traveling wave effect on the seismic response of a steel arch bridge subjected to near fault ground motions. *Earthquake Engineering and Engineering Vibration* 6(3): 246-257.
- [20] Liu Z, Zhang Z (2017) Fragility analysis of concrete-filled steel tube arch bridge subjected to near-fault ground motion considering the wave passage effect. *Smart Structure Systems* 19(4): 415-429.
- [21] Yılmaz D, Soyluk K. Dynamic Analysis of Steel Arch Bridges for Near-Fault Ground Motions Travelling with Finite Wave Velocity. *International Civil Engineering and Architecture Conference, ICEARC'19, 2019, Trabzon, Turkey.*
- [22] Boore M (2001) Effect of baseline correction on displacements and response spectra for several recordings of the 1999 Chi-Chi, Taiwan Earthquake. *Bulletin of the Seismological Society of America* 91(5): 1199-1211.
- [23] Darragh B, Silva W, Gregor N. Strong Motion Record for the PEER Center. 2018-07-11. URL: http://www.webcitation.org/query?url=http%3A%2F%2Fwww.cosmos-eq.org%2Fprojects%2Fdarragh_silva_gregor_paper.pdf&date=2018-07-11.

- [24] Dusseau AD. Unequal Seismic Support Motions of Steel Deck Arch Bridges. PhD Thesis. Michigan State University, 1985.
- [25] SAP2000, Structural Analysis Program, Version14.1, Computers and Structures Inc., Berkeley, CA.